Fault Detection in Lever-arm-compensated Position Reference Systems based on Nonlinear Attitude Observers and Inertial Measurements in Dynamic Positioning

Robert H. Rogne*, Torleiv H. Bryne†, Tor A. Johansen‡, Thor I. Fossen§,
Center for Autonomous Marine Operations and Systems
Department of Engineering Cybernetics
NTNU - Norwegian University of Science and Technology
7491 Trondheim, Norway
Email: *robert.rogne@itk.ntnu.no †torleiv.h.bryne@itk.ntnu.no ‡tor.arne.johansen@itk.ntnu.no §thor.fossen@itk.ntnu.no

***Abstract*— Marine craft employing a dynamic positioning system rely on measurements from numerous position reference systems in order to maintain the craft's desired position during operation. Faults in such systems pose a serious risk. In particular, slowly emerging faults are difficult to detect and can result in vessel drive-offs, that may in turn have dire consequences. An inertial measurement unit may provide independent position and orientation information, provided that the attitude estimates of the observer are sufficiently accurate.**

In this paper a three-stage nonlinear observer, based on strapdown inertial measurement units aided by a position reference system with uniform semiglobal exponential stability properties, is posed. The design includes lever arm compensation of position references. Fault detection is achieved with established methodology. Simulations show that this design has the potential to detect slowly emerging position reference faults.

I. Introduction

Marine craft equipped with dynamic positioning (DP) systems are subjected to a number of requirements related to sensor and positioning systems in DP Class 2 and 3 notation, to obtain resilience in single-fault scenarios [1]. An example of such requirements is the position reference (PosRef) redundancy requirement dictating that three independent PosRef systems, such as differential global navigation satellite systems (dGNSS), hydroacoustic position reference (HRP) system and taut wire, should be installed on the vessel.

Satisfying the independence condition by applying PosRefs based on different measurement principles is sometimes feasible. However, determining which PosRef is providing the most accurate position is difficult. On way to approach this problem is to install more than one PosRef system based on the same principle in order to compare the position data from each. Unfortunately, relying on more instances of a particular measurement principle entails an increased risk due to common failure modes. In the incident study [2] of DP operations, the following quote is related to dGNSS; *"six incidents are classified as drive-off, while five of these six incidents were initiated due to erroneous position data from dGPSs"*. Applying multiple dGNSS systems using the same differential link is an example of a risk inducing factor.

In order to increase the quality of PosRef fault detection and isolation, especially for faults that are not abrupt, an inertial measurement unit (IMU) can be applied.

A. Inertial Measurement Units and DP

An IMU measures linear accelerations and angular velocities. These measurements are related to position and attitude through double and single integration, respectively, in a dead reckoning (DR) fashion. While IMUs are not in widespead use in the DP industry as of today, the idea of using an IMU in conjunction with a PosRef system is not new [3], [4], [5].

Most of the literature focus their efforts on combining inertial sensors with a single PosRef system for performance reasons. The notion of utilizing an IMU for improving redundancy is far from novel [6], [7], however has had limited impact as of yet. Rogne et al. [8] investigates using IMUs as a basis for fault detection and isolation in DP. An accurate attitude estimate is of great importance when integrating the IMU's acceleration output to obtain linear velocity and position using DR. To acquire high quality estimates of the attitude, one may employ the angular velocities from the IMU, together with measurements collected from e.g. an accelerometer or compass in a sensor fusion scheme, with or without aiding from position or velocity measurements. Examples of attitude observers applying nonlinear theory are [9]-[17].

B. Lever arm compensation

Another sensor that is required for DP vessels is the vertical reference unit (VRU). Due to a DP vessel's design the respective PosRefs are located far from the nominal center of reference where the IMU may be located, as shown in Fig. 1. A distance between 30-50 meters is not uncommon. Therefore, the VRU is used to map the respective PosRefs' measurements from the measurement's location to a given point of interest utilizing roll and pitch readings provided by

This work was partly supported by the Norwegian Research Council and Rolls-Royce Marine through the MAROFF program together with the Center of Autonomous Marine Operations and Systems at the Norwegian University of Science and Technology (NTNU AMOS) (grants no. 225259 and 223254).

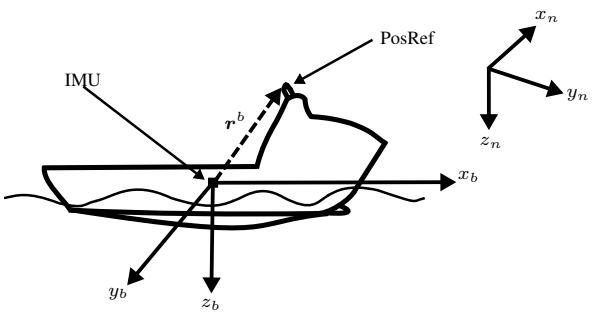

Fig. 1. Platform support vessel: Frames definition and illustration of the lever arm from IMU to a GNSS PosRef

a VRU. Since the distance between the PosRef and the point of reference can be quite large, it is most important that the roll and pitch signals from the VRU is accurate.

The approach of this paper is clearly beneficial since no assumptions on the PosRef location on the craft are needed unlike the results of [18], [12], [14], [15] where the position reference is implicitly assumed located in the same point as the IMU.

C. Main results

The main result of this paper is twofold.

- Applying a three-stage observer design with uniform semiglobal exponential stability (USGES) properties to estimate position, velocity and attitude. The lever arm between the IMU and given position reference (PosRef) system is taken into account, in contrast to previous results on nonlinear observers with USGES. Hence, the VRU is functionally embedded in the observer design, using the IMU.
- Fault detection of PosRef position measurements with slowly emerging and varying faults using fault-diagnosis techniques and the observer structure posed.

II. Preliminaries

A. General assumptions and notation

This paper employs two coordinate frames, North, East, Down (NED) and BODY, denoted $\{n\}$ and $\{b\}$, respectively as seen in Fig. 1. NED is a local Earth-fixed frame, while the BODY frame is fixed to the vessel. The origin of $\{b\}$ is defined at the nominal center of gravity of the vessel. The x-axis is directed from aft to fore, the y-axis is directed to starboard and the z-axis points downwards. A notation similar to the one in [19] is used:

- $\boldsymbol{p}^n$ - position of the vessel with respect to $\{n\}$ expressed in $\{n\}$
- $\boldsymbol{v}^n$ - linear velocity of the vessel with respect to $\{n\}$ expressed in $\{n\}$
- ψ - yaw angle between between $\{b\}$ and $\{n\}$
- $\boldsymbol{\omega}^b_{b/n}$ - body-fixed angular velocity
- $\boldsymbol{b}^b_g$ - gyro bias
- $\boldsymbol{q}^n_b$ - a unit quaternion representing the rotation between $\{b\}$ to $\{n\}$.
- $\boldsymbol{R}^n_b := \boldsymbol{R}(\boldsymbol{q}^n_b)$ and $\boldsymbol{R}^b_n := \boldsymbol{R}(\boldsymbol{q}^b_n)$ are the rotation matrices to $\{n\}$ from $\{b\}$ and vice versa, respectively. The argument $\boldsymbol{q}^n_b$ will be omitted for notational simplicity when suitable.
- $\boldsymbol{S}(\boldsymbol{x})$ - skew symmetric matrix:

$$\boldsymbol{S}(\boldsymbol{x}) = \begin{bmatrix} 0 & -x_3 & x_2 \\ x_3 & 0 & -x_1 \\ -x_2 & x_1 & 0 \end{bmatrix}, \ \boldsymbol{x} = \begin{bmatrix} x_1 \\ x_2 \\ x_3 \end{bmatrix}$$

- $\boldsymbol{g}^n$ - local gravity vector in $\{n\}$
- $\boldsymbol{f}^b_{\text{imu}}$ - accelerometer specific force measurement in the body/vessel frame $\{b\}$
- $\boldsymbol{\omega}^b_{b/n,\text{imu}} = \boldsymbol{\omega}^b_{b/n} + \boldsymbol{b}^b_g$ - angular velocity measurement of the body
- $\boldsymbol{p}^n_{\text{PosRef}}$ - position measurement
- ψ_{gc} - gyrocompass heading measurement
- p^n_I - integrated vertical position
- $\boldsymbol{c}^b = [\cos(\psi_{\text{gc}}), -\sin(\psi_{\text{gc}}), 0]^\intercal$ - vectorized compass measurement
- $\boldsymbol{c}^n = [1, 0, 0]^\intercal$ reference vector for compass

The following assumptions are made:

- IMU accelerometer biases are neglected, i.e. biases are assumed to be accounted for in calibration or by online estimation, utilizing e.g. Grip et al. [10, Sec. IV].
- There exists a bound f_{max} on the magnitude of the specific force $\boldsymbol{f}^b_{\text{imu}}$.
- $\boldsymbol{\omega}^b_{b/n}$ and $\dot{\boldsymbol{f}}^b_{\text{imu}}$ are uniformly bounded.
- To guarantee uniform observability, there exists a constant $\upsilon_{\text{obs}} > 0$ such that $\|\boldsymbol{f}^b_{\text{imu}} \times \boldsymbol{c}^b\| \geq \upsilon_{\text{obs}} \forall t \geq 0$
- We neglect measurement noise in the theoretical analysis, which is motivated by the possibility to account for noise during tuning of the observer parameters.

B. Concept

In [8], attitude estimation for use in PosRef fault detection was discussed. A main result was that a high quality attitude estimate is needed for successful IMU-based fault detection in PosRef systems. It was discovered that PosRef-aided attitude observers, such as the ones in [12], [14], [15] are excellent for fault free operation, but they are inherently vulnerable to PosRef faults. The attitude estimate should in this matter be independent from position measurements. Also, because of our intrinsic requirement that the position observer is as reliable as possible, while not filtering out information, we cannot employ observers using uncertain thrust measurements and applying wave filtering to their estimates, such as [20], [21]. Velocity measurements from PosRefs are in this design neglected since without any in-depth knowledge of how the measurement is generated, one cannot guarantee that the velocity information is independent of position. An example of such PosRefs where this might be the case is (d)GNSS.

PosRef fault detection, including lever-arm compensation, is thus done with three main components:

1) Estimating the attitude independent of the translational motion such that the innovation from a given erroneous

PosRef is not attenuated by a feedback interconnection, but still aided by a virtual reference.
2) Lever-arm-compensated translational motion estimation — mapping the PosRef measurement to the IMU's location.
3) Monitoring of the innovation signal by use of an established algorithm for detecting change in mean value.

C. System equations

The NED position of a PosRef relative a given position on the vessel is given as

$$\boldsymbol{p}^n = \boldsymbol{p}^n_{\text{PosRef}} - \boldsymbol{R}^n_b \boldsymbol{r}^b \tag{1}$$

where $\boldsymbol{r}^b$ is the lever arm as in [19, Ch. 11.5]. The kinematics of the system can be described as follows:

$$\dot{\boldsymbol{p}}^n = \boldsymbol{v}^n \tag{2a}$$
$$\dot{\boldsymbol{v}}^n = \boldsymbol{R}^n_b \boldsymbol{f}^b + \boldsymbol{g}^n \tag{2b}$$
$$\dot{\boldsymbol{q}}^n_b = \frac{1}{2}\boldsymbol{\Omega}(\boldsymbol{\omega}^b_{b/n})\boldsymbol{q}^n_b \tag{2c}$$
$$\boldsymbol{y}_p = \boldsymbol{p}^n_{\text{PosRef}} = \boldsymbol{p}^n + \boldsymbol{R}^n_b \boldsymbol{r}^b + \boldsymbol{d}_p \tag{2d}$$
$$y_\psi = \psi_{\text{gc}} = \psi + w_\psi \tag{2e}$$

where

$$\boldsymbol{\Omega}(\boldsymbol{x}) = \begin{bmatrix} \boldsymbol{0} & -\boldsymbol{x}^\intercal \\ \boldsymbol{x} & -\boldsymbol{S}(\boldsymbol{x}) \end{bmatrix} \tag{3}$$

where $\boldsymbol{d}_p$ are noise and faults on the position measurement, and w_ψ is measurement noise and faults on the gyrocompass.

III. Attitude and Heading Reference System

The methods of [12], [14], [15] estimate the position, linear velocity and attitude where the position measurements affect the attitude estimates in a feedback-interconnected structure. In this paper, the attitude is estimated independently of position measurements such that any PosRef error is prevented from propagating to the attitude estimates. The Attitude and Heading Reference System (AHRS) is however still based on the feedback-interconnected structure of [12], [14] consisting of an attitude observer, Σ_1, and an aiding translational motion observer (TMO), Σ_2 as illustrated in Fig. 2.

A. Observer equations

The attitude observer of [12], extended from [9], [10] is given as:

$$\Sigma_1 : \begin{cases} \dot{\hat{\boldsymbol{q}}}^n_b = \frac{1}{2}\boldsymbol{\Omega}(\hat{\boldsymbol{\omega}})\hat{\boldsymbol{q}}^n_b & \text{(4a)} \\ \dot{\hat{\boldsymbol{b}}}^b_g = \text{Proj}(\hat{\boldsymbol{b}}^b_g, -k_I(t)\hat{\boldsymbol{\sigma}}) & \text{(4b)} \end{cases}$$

with

$$\hat{\boldsymbol{\sigma}} = k_1 \boldsymbol{\nu}^b_1 \times \boldsymbol{R}(\hat{\boldsymbol{q}}^n_b)^\intercal \boldsymbol{\nu}^n_1 + k_2 \boldsymbol{\nu}^b_2 \times \boldsymbol{R}(\hat{\boldsymbol{q}}^n_b)^\intercal \boldsymbol{\nu}^n_2 \tag{5}$$

where

$$\boldsymbol{\nu}^b_1 = \frac{\boldsymbol{f}^b_{\text{imu}}}{||\boldsymbol{f}^b_{\text{imu}}||},\ \boldsymbol{\nu}^b_2 = \frac{\boldsymbol{f}^b_{\text{imu}} \times \boldsymbol{c}^b}{||\boldsymbol{f}^b_{\text{imu}} \times \boldsymbol{c}^b||} \tag{6a}$$
$$\boldsymbol{\nu}^n_1 = \frac{\hat{\boldsymbol{f}}^n}{\|\hat{\boldsymbol{f}}^n\|},\ \boldsymbol{\nu}^n_2 = \frac{\hat{\boldsymbol{f}}^n \times \boldsymbol{c}^n}{||\hat{\boldsymbol{f}}^n \times \boldsymbol{c}^n||} \tag{6b}$$

and $\hat{\boldsymbol{\omega}} = \boldsymbol{\omega}^b_{b/n,\text{imu}} - \hat{\boldsymbol{b}}^b_g + \hat{\boldsymbol{\sigma}}$, and $\text{Proj}(\cdot,\cdot)$ is a parameter projection that restrict the estimate $\hat{\boldsymbol{b}}^b_g$, see [10] and references therein for details.

The estimate reference vector $\hat{\boldsymbol{f}}^n = \boldsymbol{R}(\hat{\boldsymbol{q}}^n_b)\boldsymbol{f}^b_{\text{imu}} + \boldsymbol{\xi}$ is obtained by utilizing the signal ξ from a translational motion observer Σ_2 based on these kinematic equations:

$$\dot{p}^n_I = p^n_z \tag{7}$$
$$\dot{p}^n_z = v^n_z \tag{8}$$
$$\dot{\boldsymbol{v}}^n = \boldsymbol{R}^n_b \boldsymbol{f}^b_{\text{imu}} + \boldsymbol{g}^n \tag{9}$$

Furthermore, this results in the following TMO aiding the attitude observer through a feedback interconnection:

$$\Sigma_2 : \begin{cases} \dot{\hat{p}}^n_I = \hat{p}^n_z + \theta K_{p_I p_I}\tilde{p}_I & \text{(10a)} \\ \dot{\hat{p}}^n_z = \hat{v}^n_z + \theta^2 K_{p p_I}\tilde{p}_I & \text{(10b)} \\ \dot{\hat{\boldsymbol{v}}}^n = \hat{\boldsymbol{f}}^n + \boldsymbol{g}^n + \theta^3 \begin{bmatrix} 0 \\ 0 \\ K_{v p_I} \end{bmatrix} \tilde{p}_I + \theta \begin{bmatrix} K_{vv_x} & 0 & 0 \\ 0 & K_{vv_y} & 0 \\ 0 & 0 & 0 \end{bmatrix} \tilde{\boldsymbol{v}} & \text{(10c)} \\ \dot{\hat{\boldsymbol{\xi}}} = -\boldsymbol{R}(\hat{\boldsymbol{q}}^n_b)\boldsymbol{S}(\hat{\boldsymbol{\sigma}})\boldsymbol{f}^b_{\text{imu}} + \theta^4 \begin{bmatrix} 0 \\ 0 \\ K_{\xi p_I} \end{bmatrix} \tilde{p}_I + \theta^2 \begin{bmatrix} K_{\xi v_x} & 0 & 0 \\ 0 & K_{\xi v_y} & 0 \\ 0 & 0 & 0 \end{bmatrix} \tilde{\boldsymbol{v}} & \text{(10d)} \\ \hat{\boldsymbol{f}}^n = \boldsymbol{R}(\hat{\boldsymbol{q}}^n_b)\boldsymbol{f}^b_{\text{imu}} + \boldsymbol{\xi} & \text{(10e)} \end{cases}$$

with $p^n_I = 0$, and $\boldsymbol{v}^n_{\text{vir}} = \boldsymbol{0}$ such that $\tilde{p}_I = 0 - \hat{p}_I$ and $\tilde{\boldsymbol{v}} = \boldsymbol{v}^n_{\text{vir}} - \hat{\boldsymbol{v}}^n$. The virtual vertical reference (VVR) measurement, p^n_I, applied in [14], [22], is motivated by the average vertical position relative the mean sea surface is zero.

The virtual zero-velocity measurement, $\boldsymbol{v}^n_{\text{vir}}$, is a natural choice since the vessel is in stationkeeping mode where the velocity is small. In transit, the virtual velocity signals can e.g. be chosen from the desired speed s_d, obtained from the auto pilot, and the measured heading ψ_{gc} utilizing the mapping $\boldsymbol{v}^n_{\text{vir}} = [s_d \cos(\psi_{\text{gc}}),\ s_d \sin(\psi_{\text{gc}}),\ 0]^\intercal$ or velocity signals from reference models such as [19, Ch. 10] applied in DP when the vessel changes heading and position.

B. Stability of the AHRS

In Proposition 1, a USGES stability results of the AHRS is obtained by exploiting that $\Sigma_1 - \Sigma_2$ is structurally similar to the $\Sigma_1 - \Sigma_2$ of [14].

Proposition 1: The error dynamics of the observer $\Sigma_1 - \Sigma_2$ is USGES if the gain $\theta \geq 1$ is chosen sufficiently large, the gains k_1 and k_2 satisfy $k_1 \geq k_P$ and $k_2 \geq k_P$ for some

$k_P > 0$, and measurements $\boldsymbol{f}^b_{\text{imu}}$ and $\boldsymbol{\omega}^b_{b/n,\text{imu}}$ satisfy the assumptions in Sec. II-A

Proof: By defining $\tilde{p}_z := p^n_z - \hat{p}^n_z$ and $\tilde{\boldsymbol{f}} := \boldsymbol{f}^n - \hat{\boldsymbol{f}}^n$, we use that $\tilde{\boldsymbol{x}}_a := [\tilde{p}_I,\, \tilde{p}_z,\, \tilde{\boldsymbol{v}}^\intercal,\, \tilde{\boldsymbol{f}}^\intercal]^\intercal$, such that the error dynamics of (10) may be written

$$\dot{\tilde{\boldsymbol{x}}}_a = (\boldsymbol{A}_a - \boldsymbol{K}_a\boldsymbol{C}_a)\,\tilde{\boldsymbol{x}}_a + \boldsymbol{B}_a\tilde{\boldsymbol{u}}_a \tag{11}$$

where

$$\begin{aligned}\tilde{\boldsymbol{u}}_a :=\ & (\boldsymbol{I}_3 - \tilde{\boldsymbol{R}}^\intercal)\boldsymbol{R}(\boldsymbol{q}^n_b)\left(\boldsymbol{S}(\boldsymbol{\omega}^b_{b/n}) + \dot{\boldsymbol{f}}^b\right) - \\ & \tilde{\boldsymbol{R}}^\intercal\boldsymbol{R}(\boldsymbol{q}^n_b)\boldsymbol{S}(\tilde{\boldsymbol{b}})\boldsymbol{f}^b\end{aligned} \tag{12}$$

with $\tilde{\boldsymbol{b}} := \boldsymbol{b}^b_g - \hat{\boldsymbol{b}}^b_g$ and the matrices are given

$$\begin{aligned}\boldsymbol{A}_a &= \begin{bmatrix}0 & 1 & 0 & 0 & 0 & \\ 0 & 0 & 0 & 0 & 1 & \boldsymbol{0}_{2\times 3} \\ \boldsymbol{0}_{3\times 2} & & \boldsymbol{0}_{3\times 3} & & \boldsymbol{I}_3 & \\ \boldsymbol{0}_{3\times 2} & & \boldsymbol{0}_{3\times 3} & & \boldsymbol{0}_{3\times 3} & \end{bmatrix}, \\ \boldsymbol{B}_a &= \begin{bmatrix}\boldsymbol{0}_{2\times 3} \\ \boldsymbol{0}_{3\times 3} \\ \boldsymbol{I}_3\end{bmatrix}, \quad \boldsymbol{C}_a = \begin{bmatrix}1 & 0 & 0 & 0 & \dots & 0 \\ 0 & 0 & 1 & 0 & \dots & 0 \\ 0 & 0 & 0 & 1 & \dots & 0\end{bmatrix}, \\ \boldsymbol{K}_a &= \theta\boldsymbol{L}_\theta^{-1}\boldsymbol{K}_0\boldsymbol{E}_\theta,\end{aligned} \tag{13}$$

where

$$\begin{aligned}\boldsymbol{K}_0 &= \begin{bmatrix}K_{p_Ip_I} & \boldsymbol{0}_{1\times 2} \\ K_{pp_I} & \boldsymbol{0}_{1\times 2} \\ \boldsymbol{0}_{2\times 1} & \boldsymbol{K}_{a,v} \\ K_{vp_I} & \\ \boldsymbol{0}_{2\times 1} & \boldsymbol{K}_{a,\xi} \\ K_{\xi p_I} & \end{bmatrix} \\ \boldsymbol{K}_{a,v} &= \text{blockdiag}\left(K_{vv_x}, K_{vv_y}, 0\right), \\ \boldsymbol{K}_{a,\xi} &= \text{blockdiag}\left(K_{v\xi_x}, K_{v\xi_y}, 0\right),\end{aligned} \tag{14}$$

and

$$\boldsymbol{L}_\theta = \text{blockdiag}\left(1, \frac{1}{\theta}, \frac{1}{\theta^2}\boldsymbol{I}_3, \frac{1}{\theta^3}\boldsymbol{I}_3\right) \tag{15}$$

such that $\boldsymbol{E}_\theta$ satisfies $\boldsymbol{E}_\theta\boldsymbol{C}_a = \boldsymbol{C}_a\boldsymbol{L}_\theta$ and $\tilde{\boldsymbol{u}}_a$ is the perturbing term from the error dynamics of Σ_1. Since the $\boldsymbol{C}_a$ the matrix is time-invariant, its pseudoinverse $\boldsymbol{C}^\dagger$, where $\dagger$ denotes the Moore–Penrose pseudoinverse, always has full rank. $\boldsymbol{E}_\theta$ can then be calculated as $\boldsymbol{E}_\theta = \boldsymbol{C}_a\boldsymbol{L}_\theta\boldsymbol{C}^\dagger_a$. From the results of [12], extended to incorporate the VVR by [14], the feedback interconnected system of (4)–(10) requires that the matrix $(\boldsymbol{A}_a - \boldsymbol{K}_0\boldsymbol{C}_a)$ is Hurwitz and that $\theta \geq 1$ is utilized to suppress any perturbing terms form Σ_1. By defining $\boldsymbol{\eta} = \boldsymbol{L}_\theta\tilde{\boldsymbol{x}}_a$ the transformed error dynamics becomes

$$\frac{1}{\theta}\dot{\boldsymbol{\eta}} = (\boldsymbol{A}_a - \boldsymbol{K}_0\boldsymbol{C}_a)\boldsymbol{\eta} + \frac{1}{\theta^4}\boldsymbol{B}_a\tilde{\boldsymbol{u}}_a. \tag{16}$$

Since the error dynamics of (16) is equal to the corresponding error dynamics in [14, Eqs. (14)], the stability proof of [14], based on the conditions of [12], is applicable to prove that the origin of the error dynamics of the feedback interconnected system $\Sigma_1 - \Sigma_2$ is USGES. The proof in [14] involves compounded Lyapunov function candidates (LFC) for (16) and the error dynamics of (4), and dominating any indefinite terms relating the attitude and translational motion error dynamics in the compounded LFC's derivatives, using k_1, k_2 and the high-gain-like parameter θ. ■

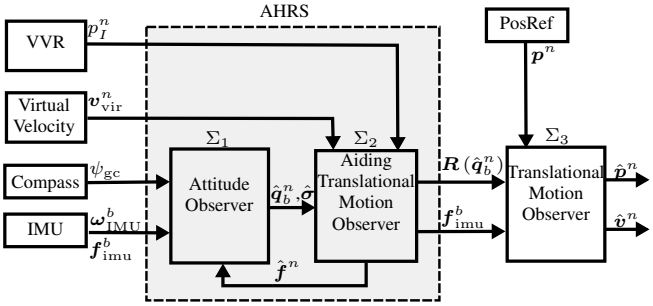

Fig. 2. Feedback-interconnected and cascaded observer structure.

IV. Lever-arm-compensated Translational Motion Observer

A. Observer equations

We employ the observer found in [19, Ch. 11] sans accelerometer bias estimation, but with the lever arm for the position measurement:

$$\Sigma_3 : \begin{cases} \dot{\hat{\boldsymbol{p}}}^n = \hat{\boldsymbol{v}}^n + \boldsymbol{K}_p\tilde{\boldsymbol{y}}_p & \text{(17a)} \\ \dot{\hat{\boldsymbol{v}}}^n = \hat{\boldsymbol{R}}^n_b\boldsymbol{f}^b_{\text{imu}} + \boldsymbol{g}^n + \boldsymbol{K}_v\tilde{\boldsymbol{y}}_p & \text{(17b)} \\ \hat{\boldsymbol{p}}^n_{\text{PosRef}} = \hat{\boldsymbol{p}}^n + \hat{\boldsymbol{R}}^n_b\boldsymbol{r}^b & \text{(17c)} \end{cases}$$

where

$$\tilde{\boldsymbol{y}}_p = \boldsymbol{p}^n_{\text{PosRef}} - \hat{\boldsymbol{p}}^n_{\text{PosRef}} \tag{18}$$

and $\hat{\boldsymbol{R}}^n_b := \boldsymbol{R}(\hat{\boldsymbol{q}}^n_b)$. With $\hat{\boldsymbol{x}} = [\hat{\boldsymbol{p}}^{n\intercal}, \hat{\boldsymbol{v}}^{n\intercal}]^\intercal$, the observer (17)-(18) can be written as:

$$\dot{\hat{\boldsymbol{x}}} = \boldsymbol{A}\hat{\boldsymbol{x}} + \boldsymbol{B}\hat{\boldsymbol{u}} + \boldsymbol{K}(\boldsymbol{y}_p - \boldsymbol{C}\hat{\boldsymbol{x}} - \boldsymbol{D}\hat{\boldsymbol{u}}) \tag{19}$$

where

$$\boldsymbol{A} = \begin{bmatrix}\boldsymbol{0} & \boldsymbol{I} \\ \boldsymbol{0} & \boldsymbol{0}\end{bmatrix}, \boldsymbol{B} = \begin{bmatrix}\boldsymbol{0} & \boldsymbol{0} \\ \boldsymbol{0} & \boldsymbol{I}\end{bmatrix}, \boldsymbol{C} = \begin{bmatrix}\boldsymbol{I} & \boldsymbol{0}\end{bmatrix}, \boldsymbol{D} = \begin{bmatrix}\boldsymbol{I} & \boldsymbol{0}\end{bmatrix}$$

and

$$\hat{\boldsymbol{u}} = \begin{bmatrix}\hat{\boldsymbol{R}}^n_b\boldsymbol{r}^b \\ \hat{\boldsymbol{R}}^n_b\boldsymbol{f}^b_{\text{imu}} + \boldsymbol{g}_n\end{bmatrix}$$

and the gain $\boldsymbol{K} = [\boldsymbol{K}^\intercal_p, \boldsymbol{K}^\intercal_v]^\intercal$ is chosen such that $\boldsymbol{A} - \boldsymbol{K}\boldsymbol{C}$ becomes Hurwitz. The terms $\boldsymbol{B}\hat{\boldsymbol{u}}$ and $\boldsymbol{D}\hat{\boldsymbol{u}}$ represent cascaded interconnections between $\Sigma_1 - \Sigma_2$ and Σ_3. The overall observer structure is found in Fig. 2

B. Stability of the Cascaded Interconnection between the AHRS $\Sigma_1 - \Sigma_2$ and TMO Σ_3

Using (2), we put the translational motion system model in the state-space representation

$$\dot{\boldsymbol{x}} = \boldsymbol{A}\boldsymbol{x} + \boldsymbol{B}\boldsymbol{u} \tag{20a}$$

$$\boldsymbol{y}_p = \boldsymbol{C}\boldsymbol{x} + \boldsymbol{D}\boldsymbol{u} + \boldsymbol{d}_p \tag{20b}$$

where

$$\boldsymbol{u} = \begin{bmatrix}\boldsymbol{R}^n_b\boldsymbol{r}^b \\ \boldsymbol{R}^n_b\boldsymbol{f}^b_{\text{imu}} + \boldsymbol{g}_n\end{bmatrix}.$$

From (20) and (17)-(19), we can derive the error dynamics for the TMO

$$\dot{\tilde{\boldsymbol{x}}} = (\boldsymbol{A} - \boldsymbol{K}\boldsymbol{C})\tilde{\boldsymbol{x}} + (\boldsymbol{B} - \boldsymbol{K}\boldsymbol{D})\tilde{\boldsymbol{u}} - \boldsymbol{K}\boldsymbol{d}_p \tag{21}$$

where $\tilde{\boldsymbol{x}} = \boldsymbol{x} - \hat{\boldsymbol{x}}$ and $\tilde{\boldsymbol{u}} = \boldsymbol{u} - \hat{\boldsymbol{u}}$.

From (21) we see that the sensor noise and faults $\boldsymbol{d}_p$ will influence the estimates, and this will be exploited in Section V to detect faults. However, for this method to be successful the nominal estimator without faults needs to be able to estimate the states in a consistent manner, so for now $\boldsymbol{d}_p$ will be neglected in order to evaluate the estimator stability.

Theorem 1: Let the gain matrix $\boldsymbol{K}$ be chosen such that $\boldsymbol{A} - \boldsymbol{KC}$ is Hurwitz, and the conditions of Proposition 1 be satisfied. If $\boldsymbol{d}_p = \boldsymbol{0}$, the origin of the error dynamics of $\Sigma_1 - \Sigma_2 - \Sigma_3$ is USGES.

Proof: Consider the nominal linear error dynamics of (21),

$$\dot{\tilde{\boldsymbol{x}}} = (\boldsymbol{A} - \boldsymbol{KC})\tilde{\boldsymbol{x}} \tag{22}$$

where the origin is GES since $(\boldsymbol{A} - \boldsymbol{KC})$ is Hurwitz. The error dynamics of (21) is perturbed by $(\boldsymbol{B} - \boldsymbol{KD})\tilde{\boldsymbol{u}}$ where the input $\tilde{\boldsymbol{u}}$ can be written as:

$$\begin{aligned}
\tilde{\boldsymbol{u}} &= \begin{bmatrix} \boldsymbol{R}_b^n \boldsymbol{r}^b - \hat{\boldsymbol{R}}_b^n \boldsymbol{r}^b \\ \boldsymbol{R}_b^n \boldsymbol{f}_{\text{imu}}^b + \boldsymbol{g}_n - \hat{\boldsymbol{R}}_b^n \boldsymbol{f}_{\text{imu}}^b - \boldsymbol{g}_n \end{bmatrix} \\
&= \begin{bmatrix} \left(\boldsymbol{R}_b^n - \hat{\boldsymbol{R}}_b^n\right) \boldsymbol{r}^b \\ \left(\boldsymbol{R}_b^n - \hat{\boldsymbol{R}}_b^n\right) \boldsymbol{f}_{\text{imu}}^b \end{bmatrix} \\
&= \begin{bmatrix} \left(\boldsymbol{I}_3 - \tilde{\boldsymbol{R}}^\intercal\right) \boldsymbol{R}_b^n \boldsymbol{r}^b \\ \left(\boldsymbol{I}_3 - \tilde{\boldsymbol{R}}^\intercal\right) \boldsymbol{R}_b^n \boldsymbol{f}_{\text{imu}}^b \end{bmatrix} = \begin{bmatrix} \tilde{\boldsymbol{u}}_1 \\ \tilde{\boldsymbol{u}}_2 \end{bmatrix}
\end{aligned} \tag{23}$$

where $\tilde{\boldsymbol{R}} = \boldsymbol{R}_b^n \left(\hat{\boldsymbol{R}}_b^n\right)^\intercal$. Taking the norm of $\tilde{\boldsymbol{u}}_1$ and $\tilde{\boldsymbol{u}}_2$ and applying that $\|\boldsymbol{R}_b^n\| = 1$, $\|\boldsymbol{I}_3 - \tilde{\boldsymbol{R}}^\intercal\| = \left\|\tilde{\eta}\boldsymbol{S}(\tilde{\boldsymbol{\varepsilon}}) - \boldsymbol{S}(\tilde{\boldsymbol{\varepsilon}})^2\right\| \leq 2\left\|\tilde{\boldsymbol{\varepsilon}}\right\|$, where $\tilde{\eta}$ is the scalar part of $\tilde{\boldsymbol{q}}$, yields:

$$\begin{aligned}
\|\tilde{\boldsymbol{u}}_1\| &= \left\| \left(\boldsymbol{I}_3 - \tilde{\boldsymbol{R}}^\intercal\right) \boldsymbol{R}_b^n \boldsymbol{r}^b \right\| \\
\|\tilde{\boldsymbol{u}}_1\| &\leq 2l\|\tilde{\boldsymbol{\varepsilon}}\|
\end{aligned} \tag{24}$$

$$\begin{aligned}
\|\tilde{\boldsymbol{u}}_2\| &= \left\| \left(\boldsymbol{I}_3 - \tilde{\boldsymbol{R}}^\intercal\right) \boldsymbol{R}_b^n \boldsymbol{f}_{\text{imu}}^b \right\| \\
\|\tilde{\boldsymbol{u}}_2\| &\leq 2f_{\max}\|\tilde{\boldsymbol{\varepsilon}}\|
\end{aligned} \tag{25}$$

where $l = \|\boldsymbol{r}^b\|$, $f_{max} = \max(||\boldsymbol{f}_{\text{imu}}^b||)$, $\tilde{\boldsymbol{\varepsilon}} = [\tilde{\varepsilon}_1 \ \tilde{\varepsilon}_2 \ \tilde{\varepsilon}_3]$ is the vector part of the error quaternion $\tilde{\boldsymbol{q}}$ associated with $\tilde{\boldsymbol{R}}$, such that if $\|\tilde{\boldsymbol{\varepsilon}}\| \to 0$ then, $\tilde{\boldsymbol{R}} \to \boldsymbol{I}_3$. While satisfying the conditions of (24)-(25), Proposition 1, and adhering to $(\boldsymbol{A} - \boldsymbol{KC})$ being Hurwitz, the GES error dynamics (22) is perturbed by the USGES error dynamics of $\Sigma_1 - \Sigma_2$ via a linearly bounded cascade connection. Then, according to Loria and Panteley [23], the error dynamics of the total system $\Sigma_1 - \Sigma_2 - \Sigma_3$ is USGES. ■

V. Fault detection

There exist numerous PosRefs available for DP. In this work we have chosen to focus on dGNSS faults, in particular non abrupt errors which in general are difficult to detect.

We have a selected a method from [24] to detect the fault itself, see below.

A. Types of faults

There are several GNSS errors that manifests themselves as faults on the GNSS receivers' outputs, like ephemeris, troposphere, satellite clock, multipath, ionosphere and receiver errors [25, Ch. 7]. Some of these may be alleviated by employing differential GNSS [25], but there are still cases where error causes faults in the receiver outputs leading to potentially dangerous situations. [26], [27] describes three manifestations as such:

- Position jump
- Slow drift
- Rapid drift

The focus of this paper will be on drifts, as detection of jumps or wild points is relatively easy and well established, see e.g. [28, Ch. 7.6].

B. Drift detection

For detecting position drifts, we will monitor the innovation signal $\tilde{\boldsymbol{y}}_p$ for any discrepancies or transients caused by $\boldsymbol{d}_p$, in a similar way as in [29] and [8]. In those papers, the TMOs were tuned so that the fault could literally be spotted by monitoring the $\tilde{\boldsymbol{y}}_p$ directly, but this caused the accuracy of the position measurement to suffer.

However, in contrast to those rather basic methods, a well established fault detection technique will be used in this paper. [24, Ch. 6.7] provides the algorithm *"CUSUM algorithm for detection of a change in the mean of a Gaussian sequence"*. The motivation for applying this algorithm is that one could reliably detect faults, while at the same time tune the observer to maintain a reasonably accurate position estimate, because of the algorithm's more sophisticated analysis of the innovation signal. Transient changes in the innovation signal as described in [29], [8], should be detected adequately by the CUSUM algorithm.

The steps in the algorithm involves:

- Initialization:
  - Assess mean and standard deviation $\tilde{\boldsymbol{y}}_p$ in fault free operation by statistical analysis of the signal.
  - Specify change of mean to be detected, as well as mean time for detection and false alarm
  - Tune the algorithm parameters to make the output comply with the detection requirements
- While running:
  - Acquire new data $\tilde{\boldsymbol{y}}_p$
  - Input new data to decision function
  - If decision function output is larger than a threshold based on the initialization, i.e. the mean has changed enough, raise an alarm.
  - Estimate time of fault occurrence

For slowly emerging PosRef faults, even minor errors in bias compensation, both for rate gyros and accelerometers, will affect the fault-detection ability since larger PosRef injection is needed if such errors sources is not compensated for sufficiently well. Also, the signal-to-noise ratio of a given PosRef measurement will affect how the decision function of the CUSUM algorithm is tuned. The algorithm must be

TABLE I

MEASUREMENT NOISES

Measurement	Std. dev.	Markov time constant
IMU acceleration	0.002 m/s^2	-
IMU gyro	0.08 deg/s	-
Position reference system x and y	1.2 m	8 min
Position reference system z	2.4 m	8 min
Gyrocompass	0.07 deg	-

able to distinguish between normal sensor output variation, and the rarer faults and drifts that may occur. A natural consequence of this is that the fault detecting abilities are limited by the noise in the nominal case.

This paper presents a fault detection strategy applicable for loosely coupled GNSS/INS integration. For tightly coupled integration strategies, other and perhaps better performing methods might be used, such as Receiver Autonomous Integrity Monitoring, known as RAIM, presented in e.g. [30, Ch. 17.4] combined with an inertial measurement unit.

VI. SIMULATION CASE STUDY

The simulations were performed in MATLAB/Simulink R2013b, making use of a dynamic ship simulator in full 6-DOF with waves [31], a simulated DP controller and added measurement noise. All measurements were set to have a zero mean normally distributed noise, except for the position reference system noise which was modeled as a Gauss-Markov process [32], see Table I for their parameters. The IMU had a sampling frequency of 100 Hz, the GNSS 1 Hz, and the gyrocompass 5 Hz. The observers in this paper were not part of the feedback loop for the DP controller. The chosen lever arm was $\boldsymbol{r}^b = [30,\ 0,\ -20]^\intercal$ corresponding to the PosRef providing measurements in a point 30 meters in front of and 20 over the IMU.

A. Observer tuning

For Σ_1 we used the gains $k_1 = 1.0, k_2 = 1.5, k_I = 0.03$. The high-gain like parameter for Σ_2 was chosen $\theta = 1$. For the gains $\boldsymbol{K}_0$ and $\boldsymbol{K}$ for Σ_2 and Σ_3, respectively, we employed the continous-time steady-state Riccati equation, similar to the Kalman-Bucy filter [33], with the following covariance matrices:

$$\begin{aligned}
\boldsymbol{Q}_{\Sigma_2} &= \text{blockdiag}(0.1^2\boldsymbol{I}_3, 0.15^2\boldsymbol{I}_3) \\
\boldsymbol{R}_{\Sigma_2} &= \text{diag}(75^2, 5^2, 5^2) \\
\boldsymbol{Q}_{\Sigma_3} &= \text{blockdiag}(\boldsymbol{0}_{3\times3}, 0.1^2\boldsymbol{I}_3) \\
\boldsymbol{R}_{\Sigma_3} &= \text{diag}(4.8^2, 4.8^2, 9.6^2)
\end{aligned}$$

For the CUSUM algorithm we set $h = 15$ and $\mu_1 = \pm 1$, where h is a tuning parameter for the algorithm sensitivity, and μ_1 is the change we want to detect. We refer to [24, Ch. 6.7, pp. 245-247] for the details of these parameters.

B. Fault free position, velocity and attitude estimation

In the first case we did a basic simulation of estimating bias, attitude, position and velocity. The results can be seen in Figs. 3 - 5. As can be witnessed, the observers managed fairly well in this task.

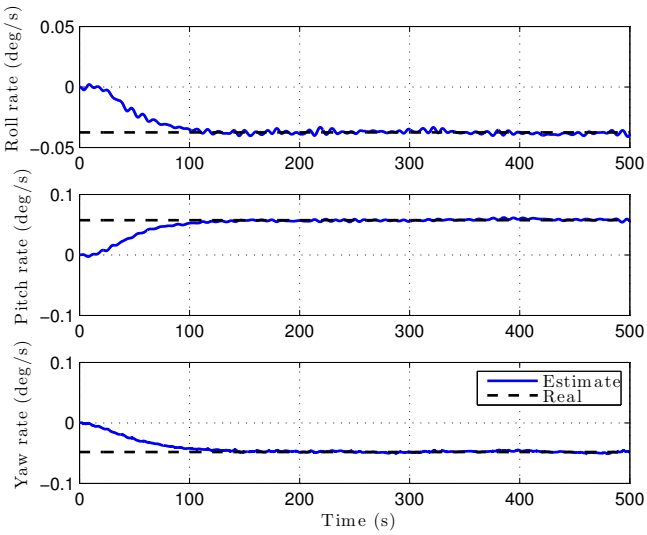

Fig. 3. Case 1 (no fault): Bias estimates

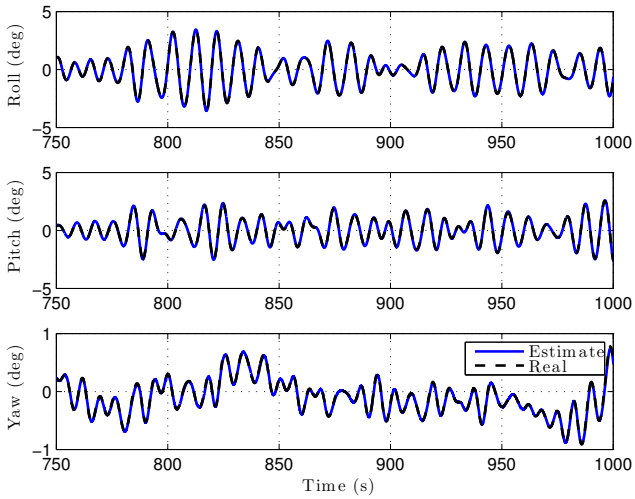

Fig. 4. Case 1 (no fault): Attitude estimates

C. Drift detection

In the second case, the position reference system was set to drift at $t = 1000s$ in the North direction with the drift shown in Fig. 6. The results are laid out in Fig. 7. As the topmost plot reveals, the position estimate followed the faulty measurement trustingly. However, the graph in the middle shows the estimation error $\tilde{\boldsymbol{y}}_{p,\text{north}}$, from which we can faintly see some spikes just after $t = 1000s$ when the drift started, and at $t = 1100s$, around the time the drift stopped. The bottom plot shows the alarm output of the CUSUM algorithm. The first alarm were raised at about $t = 1014s$, at which point the drift profile has just not yet reached 1.5 meters. The algorithm also raised an alarm at the end of the drift profile, indicating another change of mean. Furthermore,

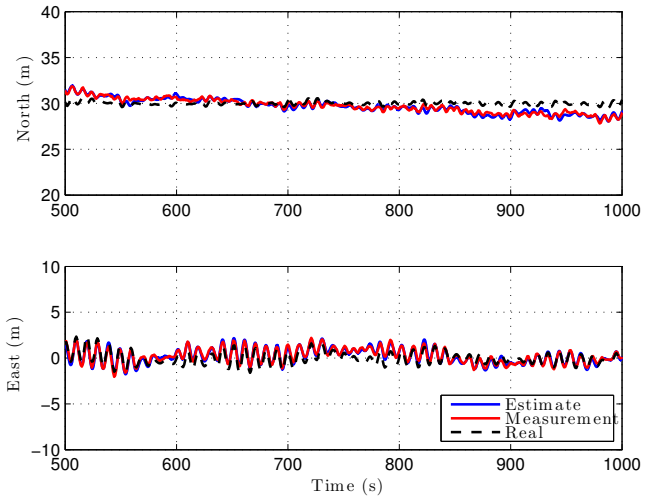

Fig. 5. Case 1 (no fault): Position estimates

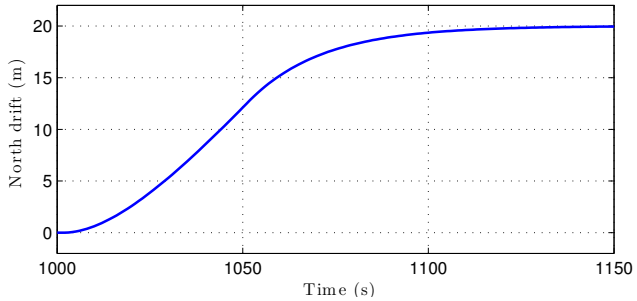

Fig. 6. Case 2: GNSS measurement drift

no false alarms were raised during the simulation run.

D. Discussion

The results of simulation Case 1 and 2 tell us that the proposed observer and fault detection scheme manages well in both disciplines — both accurate estimation and fault detection. This is in contrast to the methods in [8], [29], which had to tune their equivalent of Σ_3 very relaxed in order to catch the fault. In opposition to [8], [29], the proposed detection scheme is based on a CUSUM algorithm. To ensure that the innovation $\tilde{\boldsymbol{y}}_p$ resembles a gaussian sequence over shorter sampling intervals, the tuning of this paper is chosen to have larger feedback compared to the results [8], [29]. With a more relaxed tuning, $\tilde{\boldsymbol{y}}_p$ will resemble a Gauss-Markov process due to the simulated noise characteristics of the dGNSS. It this case, the chance of false positives might increase. Nevertheless, in a practical system, the tuning might still have to be more relaxed for robustness and sensitivity to a wider range of drift rates.

With an alarm being raised for drifting before reaching 1.5 meters, this proves that the system is a viable way of detecting faults early in the drift's progress even tough the drift scenario of this paper is seemingly more difficult, compared to those in [8], [29], since the drift in this paper is smooth, as seen in Fig 6, as opposed to a ramp shape.

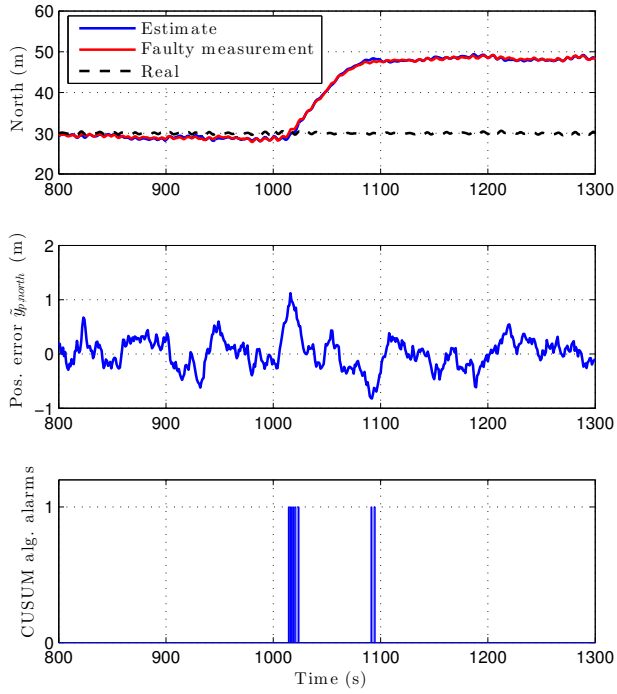

Fig. 7. Case 2: Top: Position estimate, GNSS measurement and real GNSS position. Middle: position estimate error. Bottom: CUSUM algorithm alarm output

VII. Conclusion

This paper proposed a three-stage nonlinear observer based on IMUs aided by a position reference system. The position reference system was assumed to be placed at a distance from the IMU, necessitating the need for lever arm compensation. Connecting a feedback interconnected AHRS to a translational motion observer in cascade, USGES properties were proven for the three stage observer. The observer was put in tandem with an established algorithm for fault detection, and simulations demonstrated that scheme has the capacity to detect slow drifts within a position reference system.

References

[1] *Rules for Classification of Ships, Part 6 Chapter 7. Dynamic Positioning Systems*, Det Norske Veritas, July 2013.

[2] H. Chen and T. Moan, "DP incidents on mobile offshore drilling units on the Norwegian Continental Shelf," in *Advances in Safety and Reliability - Proceedings of the European Safety and Reliability Conference, ESREL 2005*, vol. 1, 2005, pp. 337–344.

[3] Y. Paturel, "PHINS - an all-in-one sensor for DP applications," in *MTS Dynamic Positioning Conference, 28-30 September 2004, Houston, TX*, 2004.

[4] M. Berntsen and A. Olsen, "Hydroacoustic aided inertial navigation system - HAIN a new reference for DP," in *Dynamic Positioning Conference, October 9-10*, 2007.

[5] D. Russell, "Integrating INS and GNSS sensors to provide reliable surface positioning," in *Dynamic Positioning Conference October 9-10*, 2012.

[6] M. Blanke, "Diagnosis and fault-tolerant control for ship station keeping," in *Proceedings of the IEEE International Symposium on Intelligent Control, Mediterrean Conference on Control and Automation*. IEEE, 2005, pp. 1379–1384.

[7] R. Stephens, F. Crétollier, P.-Y. Morvan, and A. Chamberlain, "Integration of an inertial navigation system and DP," in *Dynamic Positioning Conference October 7 - 8*, 2008.

[8] R. H. Rogne, T. A. Johansen, and T. I. Fossen, "On attitude observers and inertial navigation for reference system fault detection and isolation in dynamic positioning," in *European Control Conference (ECC)*, Linz, Austria, July 15–17 2015, pp. 3665–3672.

[9] R. Mahony, T. Hamel, and J.-M. Pflimlin, "Nonlinear complementary filters on the special orthogonal group," *IEEE Transactions on Automatic Control*, vol. 53, no. 5, pp. 1203 – 1218, 2008.

[10] H. F. Grip, T. I. Fossen, T. A. Johansen, and A. Saberi, "Attitude estimation using biased gyro and vector measurements with time-varying reference vectors," *IEEE Transactions on Automatic Control*, vol. 57, no. 5, pp. 1332—1338, 2012.

[11] P. Batista, C. Silvestre, and P. Oliveira, "A GES attitude observer with single vector observations," *Automatica*, vol. 48, no. 2, pp. 388–395, 2012.

[12] H. F. Grip, T. I. Fossen, T. A. Johansen, and A. Saberi, "Nonlinear observer for GNSS-aided inertial navigation with quaternion-based attitude estimation," in *Proceedings of the American Control Conference*, Washington, DC, United states, 2013, pp. 272 – 279.

[13] M.-D. Hua, G. Ducard, T. Hamel, R. Mahony, and K. Rudin, "Implementation of a nonlinear attitude estimator for aerial robotic vehicles," *IEEE Transactions on Control Systems Technology*, vol. 22, no. 1, pp. 201–213, 2014.

[14] T. H. Bryne, T. Fossen, T. A. Johansen *et al.*, "Nonlinear observer with time-varying gains for inertial navigation aided by satellite reference systems in dynamic positioning," in *22nd Mediterranean Conference of Control and Automation (MED)*. IEEE, 2014, pp. 1353–1360.

[15] H. F. Grip, T. I. Fossen, T. A. Johansen, and A. Saberi, "Globally exponentially stable attitude and gyro bias estimation with application to GNSS/INS integration," *Automatica*, vol. 51, pp. 158—166, 2015.

[16] A. Khosravian, J. Trumpf, R. Mahony, and T. Hamel, "Velocity aided attitude estimation on SO (3) with sensor delay," in *IEEE 53rd Annual Conference on Decision and Control (CDC)*, 2014, pp. 114–120.

[17] M.-D. Hua, P. Martin, and T. Hamel, "Stability analysis of velocity-aided attitude observers for accelerated vehicles," *Automatica*, vol. 63, pp. 11–15, 2016.

[18] B. Vik and T. Fossen, "A nonlinear observer for GPS and INS integration," in *Proc. IEEE Conf. Dec. Cont*, vol. 3, Orlando, FL, December 2001, pp. 2956–2961.

[19] T. I. Fossen, *Handbook of marine craft hydrodynamics and motion control*. John Wiley & Sons, 2011.

[20] T. I. Fossen and J. P. Strand, "Passive nonlinear observer design for ships using lyapunov methods: full-scale experiments with a supply vessel," *Automatica*, vol. 35, no. 1, pp. 3 – 16, 1999.

[21] T. I. Fossen and T. Perez, "Kalman filtering for positioning and heading control of ships and offshore rigs," *IEEE Control Systems Magazine*, vol. 29, no. 6, pp. 32–46, 2009.

[22] T. H. Bryne, T. I. Fossen, and T. A. Johansen, "A virtual vertical reference concept for GNSS/INS applications at the sea surface," in *Proc. IFAC Conference on Manoeuvring and Control of Marine Craft*, Copenhagen, Denmark, Aug. 24–26 2015, pp. 127–133.

[23] A. Loría and E. Panteley, "Cascaded nonlinear time-varying systems: Analysis and design," in *Advanced topics in control systems theory*. Springer, 2005, ch. 2, pp. 23–64.

[24] M. Blanke, M. Kinnaert, J. Lunze, and M. Staroswiecki, *Diagnosis and Fault-Tolerant Control*, 2nd ed. Springer-Verlag Berlin Heidelberg, 2006.

[25] M. Grewal, A. P. Andrews, and C. G. Bartone, *Global navigation satellite systems, inertial navigation, and integration*, 3rd ed. John Wiley & Sons, Inc., Hoboken, New Jersey, 2013.

[26] H. Chen, T. Moan, and H. Verhoeven, "Effect of dGPS failures on dynamic positioning of mobile drilling units in the north sea," *Accident Analysis and Prevention*, vol. 41, no. 6, pp. 1164 – 1171, 2009. [Online]. Available: http://dx.doi.org/10.1016/j.aap.2008.06.010

[27] T. A. Johansen, T. I. Fossen, and B. Vik, "Hardware-in-the-loop testing of DP systems," in *MTS Dynamic Positioning Conference*, Houston, TX, November 15-16 2005.

[28] F. Gustafsson, *Statistical Sensor Fusion*, 2nd ed. Studentlitteratur, 2012.

[29] R. H. Rogne, T. A. Johansen, and T. I. Fossen, "Observer and IMU-based detection and isolation of faults in position reference systems and gyrocompass with dual redundancy in dynamic positioning," in *IEEE Multi-Conference on Systems and Control*, 2014, pp. 83 – 88.

[30] P. D. Groves, *Principles of GNSS, Inertial, and Multisensor Integrated Navigation Systems*, 2nd ed. Artech House, 2013.

[31] "MSS. Marine Systems Simulator," Viewed 20.09.2015, www. marinecontrol.org,, 2010.

[32] S. C. Mohleji and G. Wang, "Modeling ADS-B position and velocity errors for airborne merging and spacing in interval management application," *MITRE release*, 2010.

[33] R. Kalman and R. Bucy, "New results in linear filtering and prediction theory," *American Society of Mechanical Engineers – Transactions – Journal of Basic Engineering Series D*, vol. 83, no. 1, pp. 95–108, 1961.